EPR and ENDOR Studies of Deuteron Hyperfine and Quadrupole Coupling in $^{\bullet}CD(COOD)_2$: Experimental and Theoretical Estimates of Electric Field Gradients from an α-Carbon

Audun Sanderud,[†] Einar Sagstuen,*[,†] Yoshiteru Itagaki,[‡] and Anders Lund[‡]

Department of Physics, University of Oslo, P.O. Box 1048, Blindern, N-0316 Oslo, Norway, and Department of Physics and Measurement Technology, University of Linköping, S-581 83 Linköping, Sweden

Received: January 24, 2000; In Final Form: April 17, 2000

In single crystals of malonic acid grown from heavy water, the methylene protons have been partially exchanged with deuterons. Upon X irradiation at room temperature, the $^{\bullet}CD(COOD)_2$ radical is formed in an amount comparable to the $^{\bullet}CH(COOD)_2$ radical species. In the present work, EPR and ENDOR analyses of the α-deuteron hyperfine coupling (hfc) and nuclear quadrupolar coupling (nqc) tensors at room temperature have been performed. The hyperfine coupling tensor is, when scaled with the differences in the nuclear *g*-factor, almost identical to the α-proton coupling of the $^{\bullet}CH(COOH)_2$ radical at room temperature. The quadrupolar coupling tensor was found to be virtually coaxial with the hyperfine coupling tensor. The quadrupolar coupling constant is 149.8 ± 1 kHz, and the asymmetry factor $\eta = 0.092 \pm 0.020$. It is known that, at room temperature, the malonic acid radical exhibits thermal motion between two potential energy minima separated by about ±12°. Assuming that the observed hfc and nqc tensors are the result of thermal averaging between these two conformations of the radical, a simple two-site jump model was used to estimate the rigid-limit tensors. The most significant result obtained was for the nqc tensor, for which the calculations resulted in a quadrupolar coupling constant of 160 kHz and an asymmetry factor $\eta = 0.026$. These values are fairly close to the nqc parameters for the methylene deuterons in malonic acid at low temperature. The quadrupolar coupling tensor has been theoretically modeled using Slater orbitals and formal electronic populations, as well as electron populations obtained from RHF/CI INDO-type calculations. The simple model to compute the electric field gradient at the α-deuteron caused by the charge distribution at the sp^2-hybridized α-carbon was found to be as successful as more advanced methods. Furthermore, density functional theoretical (DFT) calculations for both the malonic acid radical and the native malonic acid molecule have been performed. Field gradients calculated by the DFT method significantly overestimate the quadrupolar tensors for both the α-deuteron of the radical and the methylene deuterons of the malonic acid molecule. Calculations using electron populations from the RHF/CI INDO calculations show that contributions to the quadrupolar coupling tensor from electrons and nuclei beyond the nearest-neighbor atom of the deuteron are significant.

1. Introduction

The magnetic properties of the $^{\bullet}CH(COOH)_2$ radical have been described in several electron paramagnetic resonance (EPR) and electron−nuclear double resonance (ENDOR) studies of X irradiated malonic acid derivatives,[1−5] and several theoretical analyses have been performed to properly describe the origin and characteristics of the α-proton hyperfine coupling (hfc) tensor.[4,6−8] As a consequence of this, the $^{\bullet}CH(COOH)_2$ radical has become the standard against which hundreds of observations of similar couplings have been held and scaled.[9]

Recrystallization of malonic acid from D_2O shows that the methylene protons are partly exchangeable with deuterons.[5] Similar observations were made in the case of potassium hydrogen malonate crystals.[10] The previous study[5] provided detailed information about the α-proton hyperfine coupling tensor of the $^{\bullet}CH(COOH)_2$ radical at room temperature. However, no deuteron coupling tensors were determined. In the present work, the α-deuteron hyperfine coupling tensor is determined and compared with the α-proton hyperfine coupling tensor observed by Sagstuen et al.[5]

Nuclear quadrupolar coupling (nqc) constants are commonly determined by methods such as nuclear quadrupole resonance (NQR) or nuclear magnetic resonance (NMR) spectroscopy. For various reasons,[10] these methods usually are not suitable for free radicals. Similarly, except for cases of very large couplings, the EPR technique is insensitive to quadrupole interactions. Splitting of resonance lines is, however, observed in the adjunct technique of ENDOR, and with its high resolution and relatively high sensitivity, ENDOR is particularly well suited for obtaining quadrupolar coupling tensors for paramagnetic species in diluted solids. An interesting adaptation of ENDOR is the ENDOR-detected nuclear magnetic resonance (EDNMR) technique, in which the distant ENDOR of host molecules for a paramagnetic impurity provides a sensitive tool for the study of host molecule quadrupolar couplings.[11−13]

The quadrupolar coupling constant for deuterium is small compared to that of other nuclei. This fact, combined with the general difficulty of observing deuterium ENDOR (at least in the continuous-wave (cw) mode), has led to very few reports

* Author to whom all correspondence should be addressed. E-mail: einarsa@fys.uio.no. Telephone: +47 228 55653. Fax: +47 228 55671.
[†] University of Oslo.
[‡] University of Linköping.

10.1021/jp000283h CCC: $19.00
Published on Web 06/16/2000

SCHEME 1

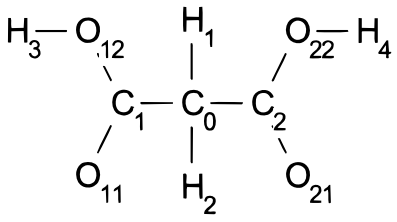

Malonic Acid

of deuterium quadrupolar coupling tensors of paramagnetic species have appeared in the literature.[10,14,15] (Note that electron spin−echo envelope modulation (ESEEM) and related time-domain techniques partly overcome this difficulty but require more sophisticated instrumentation and elaborated experimental procedures.)

In the present work, the deuterium quadrupolar coupling tensor for the α-deuterium coupling observed from the malonic acid radical formed in partially deuterated native malonic acid crystals at room temperature is reported. Assuming that the room temperature hfc and nqc tensors are the result of thermal averaging between two conformations of the radical, a simple two-site jump model was used to estimate the corresponding rigid-limit tensors. The quadrupolar coupling tensor has been theoretically modeled using Slater orbitals and electron populations obtained from INDO-type calculations, as well as density functional theory (DFT) calculations, for both the malonic acid radical and the methylene protons of the native molecule. An interesting finding is that the electric field gradient at the α-deuteron could be well modeled by the charge distribution at the sp^2-hybridized α-carbon.

2. Experimental Section

Polycrystalline malonic acid was obtained from Sigma Chemical Co. and used without further purification. Single crystals were obtained by saturating a 99.9% D_2O solution (Sigma Chemical Co.), which was stored for one week at room temperature. By this procedure, the H_1 and/or H_2 atom in a fraction of the molecules was replaced with a deuteron. The solution was then cooled to about 4 °C. With the right saturation, crystals with typical dimensions of 4−6 mm formed in less than 24 h. Malonic acid crystals are triclinic[16] with space group $P\bar{1}$ and unit cell unit parameters $a = 5.11$ Å, $b = 5.23$ Å, $c = 11.14$ Å, $\alpha = 102.7°$, $\beta = 135.17°$, $\gamma = 85.17°$, and $Z = 2$. (See Scheme 1.)

Irradiation of the crystals was done at 280 K using 40-kV, 60-mA X-rays. The doses given were approximately 30 kGy. To eliminate the other radicals present in the crystal immediately after irradiation, the crystals were kept at 340 K for about 15 hours[1] after irradiation. The crystals used for the EPR/ENDOR experiments were aligned parallel with one of the crystal axes **a**, **b**, and **c** to within 0.5°. The crystals were transferred to a quartz rod, which is a part of a one-axis goniometer, without loss of alignment. The EPR/ENDOR experiments were then performed at room temperature with the magnetic field exploring the plane perpendicular to the rotation axis, allowing for rotation of the sample through 360° to an accuracy of 0.1°.

The hyperfine and nuclear quadrupole coupling (hfc and nqc) tensors were calculated in the orthogonal system **a***, **b**′, and **c**. In terms of the cell unit vectors, $\mathbf{a}^* = \mathbf{b} \times \mathbf{c}$, and $\mathbf{b}' = \mathbf{c} \times \mathbf{a}^*$. The Eulerian angles α, β, and γ are used to specify the orientation of the magnetic field relative to the crystal. Here, α and β are equivalent to the polar angles ϕ and θ, respectively, whereas γ indicates the orientation in the plane of rotation. Simple trigonometry shows that the rotation axes can be specified in this reference system as follows: for **a**: $\alpha = -5.985°$, $\beta = 135.17°$; for **b**, $\alpha = 102.70°$, $\beta = 90°$; and for **c**, $\alpha = 0°$, $\beta = 0°$.

The crystallographic data program ORFEE[17] was used in conjunction with the neutron diffraction atomic parameters reported by McCalley and Kwiram[4] to generate inter- and intramolecular atomic contacts and their direction vectors in the ⟨**a*** **b**′ **c**⟩ reference system.

The spectrometer used for the measurements was a Bruker ESP 300E instrument optionally equipped with Bruker's DICE ENDOR unit, an ENI 3200 rf amplifier, and the Bruker ENDOR cavity. The system was set to generate a square-wave frequency modulation of the rf field at 12.5 kHz; the modulation depth used was typically 10 kHz. This small modulation depth yielded narrow ENDOR transition lines (peak-to-peak values of less than 60 kHz), which allowed for high precision in the measurements of the transition frequencies, but with accompanying loss of some signal intensity. The rf sweep width of the ENDOR spectra was 9.4 MHz, recorded at 1024 points sampling, giving a spectral resolution of 9.18 kHz.

EPR and ENDOR measurements were made by rotating the samples in 10° intervals through 180°. ENDOR line frequencies were assigned as the averaged values of the top and bottom peak value of the ENDOR lines. The low-branch lines generally exhibited low intensities and disappeared below 2.5 MHz. These lines have therefore not been used for the hfc and nqc tensor evaluations. The hfc and nqc tensors were obtained from the ENDOR data by fitting the first-order perturbation theory transition frequency expression to each individual transition.[18,19] This has been done by using a modified version of the program NQENDFIT. The program was used with the options of using an isotropic *g*-tensor and specifying the static field values at which the ENDOR spectrum was recorded, and corrections for variations in the field value were made. The theoretical values for the ENDOR transition frequencies resulting from the analyses agreed unusually well with the experimental data. The overall root-mean-square value of the fit was 6.5 kHz, and no single theoretical value differed by more than 17 kHz from the experimental data.

Semiempirical molecular orbital calculations for malonic acid were performed using the regular CNDO/2 program of Pople and co-workers[20] for closed-shell molecules and the RHF/CI INDO approach, as described by Oloff and Hüttermann,[21] for the malonic acid radical. Density functional theory (DFT) calculations were performed using the Gaussian 98[22] program package running on the Cray computer at IFM, University of Linköping. The B3LYP/6-31G protocol was used for all calculations.

3. Experimental Results

3.1. EPR. The •CD(COOD)$_2$ radical is formed by net dehydrogenation at the C_0 atom of partially deuterated malonic acid. The fraction of •CD(COOD)$_2$ radicals usually was comparable to the fraction of •CH(COOD)$_2$ radicals; however, variations occurred depending on the degree of proton/deuteron exchange at C_0. The EPR spectrum from a partially deuterated malonic acid crystal is shown in Figure 1, recorded with the magnetic field perpendicular to ⟨**a**⟩, at $\gamma = -29.4°$. This direction is close to that corresponding to the maximum α-proton/deuteron hyperfine splitting for rotation about ⟨**a**⟩. The outer major lines in the spectra, which are well described in the literature,[1,4,5] are due to the •CH(COOD)$_2$ radical. The arrows

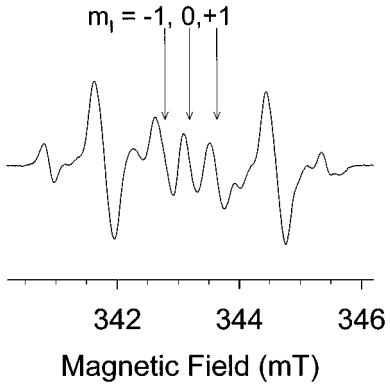

Figure 1. First-derivative EPR spectrum from a partially deuterated single crystal of malonic acid, X irradiated and measured at room temperature. The arrows indicate the three resonance lines due to the deuterium hfc. The m_I quantum numbers are assigned assuming a negative isotropic value of the deuterium hfc constant. The spectrum is recorded in the rot⟨**a**⟩-plane at $\gamma = -29.4°$, which is close to the orientation for maximum deuterium hfc splitting in this plane.

point to the three lines due to the deuteron hfc, which have been assigned m_I quantum numbers based on the assumption of a negative deuteron hfc, as observed for the corresponding proton hfc of the $^{\bullet}CH(COOH)_2$ radical.[1] Other weaker lines in the spectrum are due to other radicals.[4]

3.2. ENDOR/EIE. Because of the very small nqc of a deuteron, two ENDOR spectra were recorded for each orientation of the crystal, as illustrated in Figure 2. One spectrum was obtained with the static field locked to the high-field EPR transition (denoted $m_I = +1$ in Figure 1), yielding the $m_I = 0 \rightarrow +1$ ENDOR transition. The second spectrum used the low-field EPR resonance line (denoted $m_I = -1$ in Figure 1), yielding the $m_I = 0 \rightarrow -1$ ENDOR transitions. The m_I quantum number accompanying each line in Figure 2 refers to the EPR line to which the magnetic field is locked.

The two spectra obtained differ because of different m_I ENDOR transitions, as shown in Figure 2. Because the $m_I = +1$, $m_s = +^1/_2$ ENDOR line transition frequency is higher than that of the $m_I = -1$, $m_s = +^1/_2$ line, it is concluded that the nqc must have the same sign as the hfc at this orientation. The hfc and nqc tensors given in Table 1 were calculated from the data shown in Figure 3, assuming the m_I and m_s assignments shown in Figure 2 as well as a negative deuteron hfc.

At the right in Figure 2, the EIE (ENDOR-induced EPR) spectra from the four ENDOR lines are shown. This procedure demonstrates that the two EPR lines associated with the $m_I = \pm 1$ quantum numbers induce the ENDOR spectra associated with the same m_I values and confirms the m_I and m_s quantum number assignments of the EPR and ENDOR lines.

The starting orientations for the three axes of rotation, corresponding to $\gamma = 0$, were not found by X-ray diffraction. Therefore, the following procedure was applied: For a given axis of rotation, two directions are common with one from each of the other two axes. For example, for rot⟨**a**⟩, the two directions are those corresponding to $\pm\langle \mathbf{b}^* \rangle$ and $\pm\langle \mathbf{c}^* \rangle$ (in terms of unit vectors, $\mathbf{b}^* = \mathbf{c} \times \mathbf{a}$ and $\mathbf{c}^* = \mathbf{a} \times \mathbf{b}$). The angle between these common directions, A, is given by the relationship $\cos A = (\cos \alpha - \cos \beta \cos \gamma)/(\sin \alpha \sin \beta)$. It is found that the angles between the common directions are as follows: rot⟨**a**⟩, 45.28°; rot⟨**b**⟩, 103.18°; and rot⟨**c**⟩, 95.99°. With this information, the positive direction of rotation about each of the three rotation axes is fixed. By assigning start values of γ so that the common orientations were approximately aligned and then allowing for optimization with respect to best fits to the experimental data using the program NQENDFIT,[19] we were able to determine the γ values to an accuracy of 0.01°.

Figure 3 shows the angular variation of the experimental ENDOR transition frequencies of the deuterium coupling in all three planes of rotation, together with those calculated using the tensor parameters given in Table 1. Only the high-frequency branch of the experimental data was used for the analysis.

3.3. Thermal Effects. In a previous ENDOR work on malonic acid,[4] it was shown that, at 4.2 K, the malonic acid radical exists in two conformations. The C_0-H fragment occupies one of two possible conformations, rotated ±12° about the C_1-C_2 direction. At room temperature, the single RCHR radical observed[5] must be assumed to exhibit a motionally averaged proton hfc tensor due to a rapid interconversion between the two potential minima at ±12°.

As a consequence of this, the hfc and nqc tensors determined in the present and previous[5] works represent thermal averages of the "true" rigid-limit couplings. Proton hyperfine coupling tensors of the malonic acid radical were determined by McCalley and Kwiram at 4.2 K.[4] On the other hand, the corresponding nqc tensors have not been measured. It would be of interest to estimate the rigid-limit nqc tensors for later comparison and analysis.

Consider a librational movement spanning an angle of $\pm\theta$ about an equilibrium angle $\theta_0 = 0°$. If the axis of libration is about the C_1-C_2 direction,[4] y (= y') in Figure 5, and the rigid-limit coupling principal axes are designated z' (along the C_0-D bond) and x' (perpendicular to the radical plane), then the averaged coupling principal values are[23]

$$T_{zz} = T_{z'z'}\langle \cos^2 \theta \rangle + T_{x'x'}\langle \sin^2 \theta \rangle$$

$$T_{xx} = T_{z'z'}\langle \sin^2 \theta \rangle + T_{x'x'}\langle \cos^2 \theta \rangle$$

where ⟨ ⟩ symbolizes a dynamical average. The actual values of these averages depend on the distribution of conformations. Two typical simple examples are a two-site jump model and a continuous distribution function with equal weight at each orientation. For the two-site model,[24]

$$\langle \cos^2 \theta \rangle = {}^1/_2[1 + \cos(2\theta)]; \quad \langle \sin^2 \theta \rangle = {}^1/_2[1 - \cos(2\theta)]$$

whereas for an equal-weight continuous distribution function, we have[25]

$$\langle \cos^2 \theta \rangle = {}^1/_2[1 + \sin(2\theta)/2\theta]; \quad \langle \sin^2 \theta \rangle = {}^1/_2[1 - \sin(2\theta)/2\theta]$$

In the present case, it appears as if the two-site jump model is the most relevant model for the actual rapid averaging motion of the α-proton between the two minimum positions. Using $\theta = 12°$,[4] we obtain for the rigid-limit proton hfc, principal values of (−90.25, −57.90, −26.04) MHz; for the deuteron hfc principal values of (−14.073, −8.979, −4.157) MHz; and for the deuteron nqc tensor, principal values of (80.0, −41.1, −39.0) kHz. These results will be further discussed below.

Larger thermal amplitudes at room temperature may further modulate the libration of the C_0-D fragment. This can be modeled by also adding contributions using a continuous distribution function. Precise measurements of the C_0-D hfc and nqc tensors at low temperatures are necessary for this to be a useful exercise.

4. Calculation of the Deuteron Nuclear Quadrupolar Interaction

4.1. Theory. The nuclear quadrupolar interaction can be expressed as a tensor coupling of the nuclear spin with itself,[26]

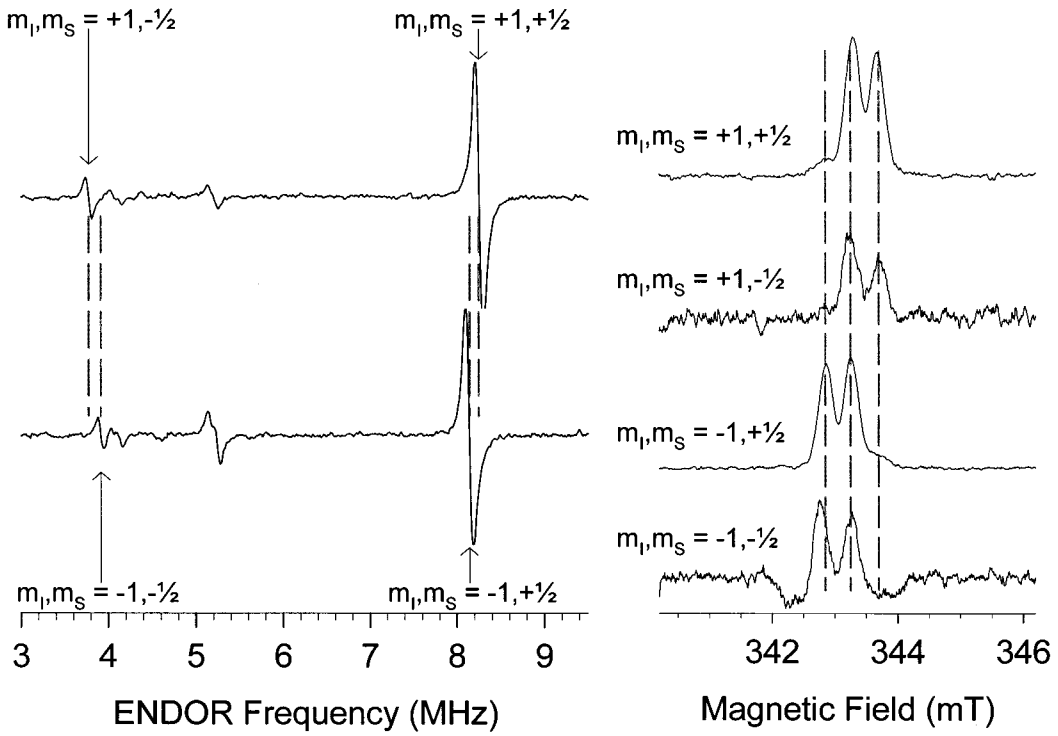

Figure 2. Left: Two ENDOR spectra from a partially deuterated malonic acid single crystal, X irradiated and measured at room temperature. The spectra are recorded at the same orientation as for the EPR spectrum in Figure 1 with the magnetic field locked to the EPR lines designated with $m_l = +1$ and -1, as shown. The ENDOR resonance lines associated with the deuterium hyperfine coupling are marked with m_s quantum numbers assuming a negative isotropic value of the deuterium hyperfine coupling constant. Right: The four EIE spectra recorded from the four different ENDOR lines associated with the deuterium hfc. The spectra are assigned with the respective quantum numbers. Both the ENDOR and the EIE spectra show that the signs of the hyperfine and quadrupolar coupling are the same at this orientation of the crystal.

TABLE 1: Experimental Deuterium Hyperfine Coupling and Nuclear Quadrupolar Coupling Tensors for the •CD(COOD)$_2$ Radical in Malonic Acid[a]

	principal values (MHz)			eigenvectors		
tensor	A	a_{iso}	B	**a***	**b**′	**c**
Dα	−4.365(5)	−9.070	4.705	−0.0875	0.9086	−0.4100
	−8.771(3)		0.299	0.9954	0.0640	0.0708
	−14.073(6)		−5.003	0.0380	0.4144	0.9093
Q(D)	0.0749(11)			−0.1556	0.9084	−0.3880
	−0.0339(10)			0.9770	0.0837	−0.1960
	−0.0411(10)			0.1456	0.4096	0.9006

[a] Numbers in parentheses are uncertainties in the last significant digit(s) of the corresponding number.

$H_q = \mathbf{I}\cdot\hat{\mathbf{Q}}\cdot\mathbf{I}$, where the quadrupolar coupling tensor $\hat{\mathbf{Q}}$ is given by the elements

$$Q_{ij}\,(\mathrm{Hz}) = \frac{eQ}{2I(2I-1)h}\frac{\partial^2 V}{\partial x_i \partial x_j} \qquad (1)$$

where Q is the nuclear quadrupole moment. $\partial^2 V/\partial x_i \partial x_j$ are the elements of the electric field gradient tensor at the quadrupole, expressed by the electrostatic potential V. The contribution to the electric field gradient tensor from a single particle of charge q at a distance r from the quadrupole is then

$$\frac{\partial^2 V}{\partial x_i \partial x_j} = \frac{\partial^2}{\partial x_i \partial x_j}\frac{q}{4\pi\epsilon_0 r} = \frac{q}{4\pi\epsilon_0}\frac{3x_i x_j - \delta_{ij} r^2}{r^5} = \frac{q}{4\pi\epsilon_0}P_{ij}(r) \qquad (2)$$

If an atomic nucleus is considered to be a point charge with formal charge equal to the atomic number, then this is the contribution to the elements $\partial^2 V/\partial x_i \partial x_j$ from one of the nuclei surrounding the quadrupole. As for the electrons, their distribution is described by molecular orbitals ψ_k. The electric field gradient tensor elements can then be constructed as the sum of contributions from all of the nuclei l and all of the molecular orbitals k.

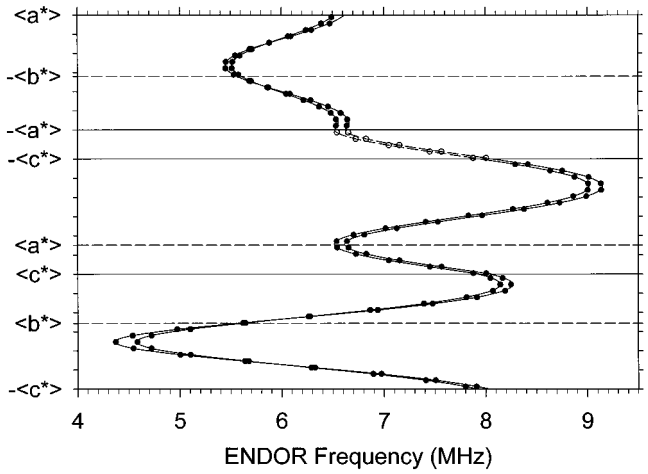

Figure 3. Angular variation of the ENDOR transitions of the deuterium coupling in the •CD(COOD)$_2$ radical measured at room temperature. The solid lines represent the angular variation with the magnetic field locked at 343.46 mT, calculated from the tensors listed in Table 1. The ENDOR data points are recorded at different magnetic fields, with variations up to 1.2 mT from this average value.

$$\frac{\partial^2 V}{\partial x_i \partial x_j} = \sum_l \frac{q_l}{4\pi\epsilon_0}P_{ij}(r_l) - \sum_k \frac{e}{4\pi\epsilon_0}\langle\psi_k|P_{ij}(r)|\psi_k\rangle \qquad (3)$$

When the molecular orbitals are approximated by a linear combination of atomic orbitals, $\psi_k = \sum_\mu a_{\mu k}\varphi_\mu$, the electron part

of eq 3 can be expressed in terms of the charge density matrix elements $\rho_{\mu\nu}$ and integrals over the atomic orbitals.

$$\langle P_{ij}\rangle = \sum_k \langle \psi_k | P_{ij}(r) | \psi_k \rangle = \sum_{\mu\nu} \sum_k a_{\mu k} a_{\nu k} \langle \varphi_\mu | P_{ij}(r) | \varphi_\nu \rangle = \sum_{\mu\nu} \rho_{\mu\nu} \langle \varphi_\mu | P_{ij}(r) | \varphi_\nu \rangle \quad (4)$$

Townes and Dailey[27] argued that only contributions from electrons at the center atom exhibiting a nuclear quadrupolar moment should be taken into account. For the D atom, however, there is no field gradient due to the $|1s\rangle$ orbital located at the deuteron. Hence, to describe the nqc observed for the •CD(COOD)$_2$ radical, the nuclei and charge density elsewhere in the molecule must be taken into account. The major contribution to the quadrupolar tensor is from C_0 because of the $1/r^3$ dependence of the quadrupolar tensor elements (eq 3). By describing the electron distribution with Slater orbitals at a carbon atom located a distance R from the quadrupole, it is possible to calculate the contributions to the electric field gradient tensor elements P_{ij} from each electron. The integrals involved are of the same type as those used to evaluate anisotropic hyperfine couplings. The integrals of relevance to carbon-centered radicals were first evaluated by McConnell and Strathdee.[7] Corrected and extended lists have been published by Barfield,[28] Beveridge and McIver,[29] and Edlund et al.[30] These authors have taken into account the contributions caused by the cusps in the Slater orbitals,[28,31] which were ignored in the initial calculations by McConnell and Strathdee.[7] However, the latter formulas (corrected for minor errors[28]) have most commonly been used to investigate hfc tensors and have proven to yield satisfactory agreement with experimental hfc data for π-electron radicals.[32] In this case, only integrals of the type $\langle 2p_x | P_{ii}(r) | 2p_x \rangle$ were required. To obtain the nqc tensor, several more integrals are needed. The cusp contributions were disregarded also in this instance. This method using Slater orbitals to calculate the nqc tensor does not seem to have received much attention. The relevant integrals are therefore given in Appendix A.

4.2. The Malonic Acid Radical. In the first model, sp^2 hybridization is assumed at C_0, with an electron configuration $(1s)^2(2sp^2)^3(2p_x)^1$. The x axis is perpendicular to the radical plane. The sp^2 hybrids are directed along the z axis, and symmetrically disposed about the negative z axis in the yz plane, respectively. The contribution from the electrons at C_0 to the deuteron nqc tensor was calculated to be

$$\langle P_{ij}\rangle = 2\langle 1s | P_{ij}(r) | 1s \rangle + \langle 2s | P_{ij}(r) | 2s \rangle + \langle 2p_x | P_{ij}(r) | 2p_x \rangle + \langle 2p_y | P_{ij}(r) | 2p_y \rangle + \langle 2p_z | P_{ij}(r) | 2p_z \rangle \quad (5)$$

Because of the symmetry of the sp^2 orbitals, the charge density elements $\rho_{\mu\nu} = 0$ for atomic orbitals $\mu \neq \nu$. Furthermore, all elements with $i \neq j$, $i = x$, y, or z vanish. The carbon nucleus has $q = +6$, and each of the 1s contributions is assumed to be that of a point charge (which is an overestimation of less than 3×10^{-9} Hz when the values of $R = 1.0$ Å for the C_0−D bond length and $Z^* = 5.7$ are used). Using the integrals in Appendix A, eq 3 can be expressed as

$$\left[\frac{12}{R^3} - \langle P_{zz}\rangle\right] = \frac{8e^{-2a}(^2/_3 a^4 + {}^4/_3 a^3 + 2a^2 + 2a + 1)}{R^3}\left[-\frac{6}{R^3} - \langle P_{xx}\rangle\right] = \left[-\frac{6}{R^3} - \langle P_{yy}\rangle\right] = -\frac{1}{2}\left[\frac{12}{R^3} - \langle P_{zz}\rangle\right] \quad (6)$$

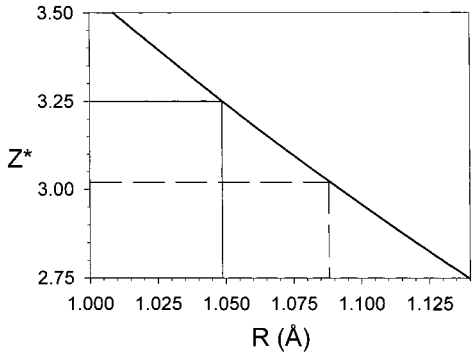

Figure 4. Effective nuclear charges Z^* for the carbon 2s and the 2p orbitals plotted as a function of distance R between the D and C_0 atoms, to obtain a solution of eq 7 that gives a theoretical nqc tensor with $Q_{zz} = 80.0$ kHz, equal to the estimated rigid-limit value. The solid lines show that, with $Z^* = 3.25$, the distance $R = 1.049$ Å must be chosen. The dashed lines show that, using $R = 1.088$, the effective nuclear charge for the 2s and 2p orbitals becomes $Z^* = 3.03$.

With R expressed in units of the Bohr radius a_0 (that is, in au), as in Appendix A, and with the deuteron nuclear quadrupole moment $Q = 28.75 \times 10^{-24}$ m^2,[33] the factor $e^2Q/4\pi\epsilon_0 2I(2I-1)ha_0^3$ equals 337.8 kHz. Multiplying this factor by eq 6 gives the quadrupolar tensor elements expressed in kHz.

$$Q_{zz}\,(\mathrm{kHz}) = \frac{eQ}{4\pi\epsilon_0 2I(2I-1)ha_0^3} e^{-Z^*R}\left(\frac{Z^{*4}R}{3} + \frac{4Z^{*3}}{3} + \frac{4Z^{*2}}{R} + \frac{8Z^*}{R^2} + \frac{8}{R^3}\right) \quad (7)$$

$$Q_{xx}\,(\mathrm{kHz}) = Q_{yy}\,(\mathrm{kHz}) = -{}^1/_2 Q_{zz}\,(\mathrm{kHz})$$

Equation 7 has two unknown parameters, the distance R between C_0 and D and the effective nuclear charge Z^* for the 2s and 2p orbitals. In Figure 4, Z^* is plotted as a function of R to obtain a solution of eq 7 yielding a theoretical nqc tensor with Q_{zz} equal to the estimated rigid-limit value of 80.0 kHz. The effective nuclear charges Z^* are suggested[20] to be 5.7 for the carbon 1s orbital and 3.25 for the carbon 2s and 2p orbitals. With these values, the distance $R = 1.049$ Å must be chosen (as shown by the solid line in Figure 4) to give a theoretical nqc tensor with Q_{zz} equal to the estimated rigid-limit value of 80.0 kHz. The value $R = 1.088$ Å was used in previous papers[7,29] to theoretically calculate the α-proton dipolar hfc in •CH(COOH)$_2$. The dashed curve in Figure 4 shows that, using this R value, the effective nuclear charge for the 2s and 2p orbitals becomes $Z^* = 3.03$ if the theoretical nqc tensor is modeled with Q_{zz} equal to the estimated rigid-limit value. In the remainder of this work, the deliberate choice was made to use the standard values of R and Z^* (1.088 Å and 3.25, respectively[20]). The above discussion, however, makes it clear that this will lead to a significant underestimation of the nqc tensor when compared to the estimated rigid-limit tensor.

The contribution from C_0 to the deuteron nqc tensor was calculated as described above. In addition, a planar $>C_0$−D fragment was assumed, as estimated from crystallographic data and an assumption of sp^2 rehybridization at C_0 upon net hydrogen abstraction from that position. The numerical values are listed in Table 2 as Tensor **I**. As expected, the magnitudes of the principal values are somewhat too low.

In a more refined molecular model, the valence orbitals are not expected to possess the formal electron populations. A simple way of estimating the valence electron populations of the orbitals describing the electron distribution in a radical is

TABLE 2: Estimated Deuterium Nuclear Quadrupole Coupling Tensors for the • CD(COOD)$_2$ Radical and for the Methylene Deuterons of Deuterated Malonic Acid[a]

		principal values (kHz)		
tensor	method of estimation	x	y	z
	•CD(COOD)$_2$, experimental	−33.9	−41.1	74.9
	•CD(COOD)$_2$, rigid-limit model	−39.0	−41.1	80.0
I	C_0−D fragment[b,c]	−31.7	−31.7	63.4
II	C_0−D fragment[b,d]	−27.0	−28.9	55.9
III	•CD(COOD)$_2$[b,d]	−29.9	−29.7	59.6
IV	•CD(COOD)$_2$[e]	−57.2	−51.0	108.2
	malonic acid, D1, exp.[f]	−43.7	−40.5	84.2
	malonic acid, D2, exp.[f]	−44.7	−40.7	85.4
V	malonic acid, D1[b,g]	−33.1	−33.1	66.2
VI	malonic acid, D2[b,g]	−33.1	−31.1	64.2
VII	malonic acid, D1[e]	−57.0	−52.6	109.6
VIII	malonic acid, D2[e]	−57.1	−52.8	109.9

[a] All of the tensors estimated are coaxial or within 1° from the basis (x, y, z) defined as x || (C_0−D) × (C_1−C_2), z || C_0−D, and y || (C_1−C_2), which gives x || LEO in the •CD(COOD)$_2$ radical. [b] Slater orbitals. [c] Unit electron population in the orbitals. [d] Electron populations calculated using the RHF/CI INDO method. [e] Electric field gradient tensor calculated with DFT. [f] β phase, T = 65 K.[13] [g] Electron populations calculated using the CNDO/2. method.

to use the INDO RHF/CI semi-empirical approach described by Oloff and Hüttermann[21] in a geometry based on crystallographic data. When the total charge density matrix elements around C_0 obtained from such calculations are used in eq 4, Tensor **II** in Table 2 is obtained. The absolute values of all of the quadrupole tensor principal elements have been reduced. This is because of the total electron population at C_0 being calculated to be 6.16. The RHF/CI INDO result also shows that, for the two other carbon atoms (C_1 and C_2), there are corresponding reductions in total electron population.

In a third model, the contributions to the deuteron quadrupolar coupling tensor from each atom in the malonic acid radical were calculated based on the RHF/CI INDO-calculated density matrix and added together in the basis defined by the hyperfine coupling tensor. The resulting Tensor **III** is shown in Table 2. This tensor exhibits principal directions deviating by less than 1° from the basis described in Table 2. The magnitudes of the tensor elements have increased slightly relative to those of Tensor **II**. The tensor is close to being axially symmetric.

The last model is based on density functional theory (DFT). DFT methods are known to give more accurate estimates of hyperfine coupling constants of radicals than INDO-based methods. It might be expected that this protocol also yields more accurate electron distributions. The Gaussian 98 program, in addition, allows for the geometrical structure of the molecule or radical to be optimized. In this work, only the geometry about C_0 of the radical has been optimized so that the original angle of twist between the two carboxyl groups and the two intermolecular hydrogen bonds in the single crystal is conserved.[16] All details of these DFT calculations are provided by Sagstuen et al.[5] Gaussian 98 has a function for calculating the electron field gradient tensors. This function was used, and the resulting deuteron quadrupolar tensor is shown as Tensor **IV** in Table 2. This tensor also deviates by less than 1° from the hfc tensor basis in Table 2; however, the quadrupolar coupling tensor elements are about 35% larger in magnitude than those of the estimated rigid-limit nqc tensor. The tensor is asymmetric but apparently in a direction opposite to that of the experimentally obtained as well as the rigid-limit-estimated tensors.

4.3. Quadrupolar Interaction in the Undamaged Molecule. McCalley and Kwiram[11] and Krzystek et al.[13] have determined the deuteron quadrupolar coupling constants for the methylene deuterons of perdeutrated malonic acid using EDNMR. The nqc tensor principal values shown in Table 2 are from the work of Krzystek et al.,[13] recorded at 65 K, which is above the $\gamma-\beta$ phase transition of the malonic acid crystal.

In malonic acid, the central carbon C_0 exhibits sp^3 hybridization, but because of the symmetry of the molecular orbitals, the charge density elements $\rho_{\mu\nu} = 0$ for atomic orbitals $\mu \neq \nu$. Hence, from eq 4, the resulting contribution to the field gradient is the same as that for the •CD fragment with sp^2 hybridization, as shown in eq 5. This simple calculation, therefore, does not account for the apparent difference between the nqc tensors of the methylene deuterons of malonic acid and the α-deuteron of the malonic acid radical. A difference may be expected because of the additional hydrogen atom present in the undamaged molecule. This atom will not contribute to the electric field gradient at the deuteron provided that there is one electron in the 1s orbital. However, a minor reduction of the electron charge density in the 1s orbital will give a contribution that increases the magnitude of the calculated nqc tensor elements. Also, the limitations of the crude model used to estimate the rigid-limit nqc tensor elements must be kept in mind.

Additionally, the CNDO/2 method was used to estimate the electron charge density matrix for the molecule. Using this matrix, the resulting quadrupolar tensor (Tensor **V** in Table 2) was obtained for a deuteron located at the H_1 atom position in the malonic acid molecule, whereas Tensor **VI** is the estimate obtained for the deuteron in the H_2 position. The electric field gradients from DFT calculations for the fully optimized malonic acid molecule were also used. These yield, for the deuteron at the H_1 position, Tensor **VII** and, for the deuteron at the H_2 position, Tensor **VIII**. All of these tensors have principal axes that deviate less than 1° from the basis described in Table 2.

5. Discussion of the Experimental Hyperfine Coupling Tensors

The radical •CD(COOD)$_2$ is the result of a net dehydrogenation/dedeuteration of malonic acid. The eigenvector for the intermediate principal value is expected to be parallel to the lone-electron orbital (LEO) and, for a π-electron radical, directed along the normal of the $C_1-C_0-C_2$ plane.[7] The experimental value listed in Table 1 deviates just 5.8° from the normal of this plane, as calculated from the crystallographic data. The eigenvector for the minimum principal value is expected to be directed parallel to the $>C_0-D$ bond direction estimated as the in-plane bisector of the angle $C_1-C_0-C_2$. However, the experimental eigenvector deviates 23.0° from the corresponding crystallographic direction. The D atom appears to be located closer to the initial position of C_1 than to that of C_2. This was also observed in the case of the •CH(COOH)$_2$ radical in the previous work on malonic acid.[5] As discussed in that study, it is assumed that this deviation results from a slight conformational change in the $C_1-C_0-C_2$ backbone upon radical formation.

McConnell and co-workers[6,7] have made quantitative calculations of both the isotropic and anisotropic part of the hyperfine tensor of an α-proton tensor. The isotropic part, α_{H_μ}, has been described with the so-called McConnell[34] equation

$$\alpha_{H_\mu} = Q^{H}_{CH}\rho_\mu \tag{8}$$

where ρ_μ is the π-spin density of the LEO at atom μ.

For the RC−CH−CR fragment, the proportionality constant $Q^{H}_{CH} = -73.4$ MHz,[35] and with $g_D\beta_D/g_H\beta_H = 0.1535$, $Q^{D}_{CD} = -11.3$ MHz. With an isotropic value of −9.070 MHz (Table

1), this model gives a spin density of $\rho_{LEO} = 0.80$, which is the same as that estimated for the $^{\bullet}CH(COOH)_2$ radical.[4,5]

Assuming that the room-temperature hfc tensors are the result of thermal averaging between two conformations of the radical, the simple two-site jump model used to estimate the rigid-limit tensors above indicates that, for the hyperfine coupling tensors, the effect of libration is small. Most notably, however, the intermediate dipolar hfc principal values becomes very close to zero (0.16 and 0.09 MHz for the proton and deuteron hfc tensors, respectively), in agreement with the previous low-temperature measurements of the rigid-limit hfc proton tensors.[4]

6. Discussion of the Deuteron Nuclear Quadrupole Tensor

6.1. Experimental nqc Tensor. The experimental nqc tensor is close to being axially symmetric. According to conventional notations,[36] the quadrupolar coupling constant $e^2Qq = 149.8 \pm 1$ kHz, and the asymmetry coefficient $\eta = 0.096 \pm 0.020$. The nqc tensor is almost coaxial with the hfc tensor, with the nqc symmetry axis expressed by the eigenvector associated with the positive principal value only 3.6° from the apparent $>C_0-D$ direction of the hfc tensor (the eigenvector for the minimum principal value).

Assuming that the room-temperature nqc tensor is the result of thermal averaging between two conformations of the radical, the simple two-site jump model used to estimate the rigid-limit tensor above (reproduced in Table 2) indicates a significant effect of libration on the nqc tensor principal values. The quadrupolar coupling increases to $e^2Qq = 160.0$ kHz, whereas the anisotropy decreases to $\eta = 0.026$. From the data listed in Table 2, it is clear that the calculated rigid-limit values above are quite close to the nqc constants measured for the C_0-D deuterons in malonic acid (β phase, T = 65 K[13]). Colligiani et al.[10] determined the room-temperature α-deuteron hfc and nqc tensors for the radical $^{\bullet}CD(COO^-)_2$ formed by X irradiating potassium hydrogen malonate crystals. The principal values of the nqc tensor were determined to be (−47.5, −43.0, 86.5) kHz ($e^2Qq = 173$ kHz, $\eta = 0.052$), with the asymmetry related to the hfc tensor principal axes similar to that observed in the present work. Unfortunately, this tensor is quite far from being traceless.

6.2. Calculated nqc Tensor. In our attempts to model the experimental nqc tensor with different calculational methods, we find that the simplest method, with a $(1s)^2(2sp^2)^3(2p_x)^1$ electron configuration described by Slater orbitals and with only the C_0-atom contributions taken into account (Tensor **I** in Table 2), gives surprisingly good agreement with experimental data considering the limitations imposed. Tensor **III**, obtained by taking electron populations determined by RHF/CI INDO calculations at all atoms of the malonic acid radical, gives a similarly acceptable result. A consideration of the difference between Tensor **II** and Tensor **III** indicates that the distant atoms and electrons contribute only about 5% of the magnitude of the positive principal value.

The DFT method overestimates the nqc tensor elements significantly. The optimized bond length of the $D-C_0$ bond is 1.083 Å, close to the value 1.088 Å used for calculating Tensors **I**, **II**, and **III**, and thus, it will not contribute significantly to the difference in results. A possible explanation is that the orbital basis used for the calculations (6-31G) allows for electron density in 3s and 3p orbitals at carbon and oxygen atoms. The different electron orbital contributions described in Appendix A all yield components to the nqc tensor that are opposite in sign to the contributions from the positively charged nucleus. In Tensor **I**, which has contributions from an equal amount of positive and negative charge, the net quadrupolar coupling is due to the contributions from the electrons being smaller in magnitude because of their spatial distribution. The magnitude of the quadrupolar tensor elements will increase further if the electron spatial distribution is further increased, which can indeed occur in the DFT calculations by populating the 3s and 3p orbitals. The output from the DFT calculations shows that the total electron population of C_0 orbitals is 6.053, of which 1.288 is assigned to 3s or 3p orbitals.

The nqc tensors of the methylene deuterons of perdeutrated malonic acid observed by Krzystek et al.[13] are about 6% larger than the estimated rigid-limit nqc tensor for the malonic acid radical in the present work. The corresponding nqc tensors **V** and **VI** calculated using electron populations obtained from the CNDO/2 calculations are about 10% larger in magnitude than Tensor **III**, calculated for the malonic acid radical case. On the other hand, the DFT calculations give quadrupolar coupling tensors with small differences between the two cases of undamaged molecule and radical.

Acknowledgment. Thanks are due to Prof. Willam H. Nelson for his help with the ORFEE calculations. Dr. Anders R. Sørnes is acknowledged for making the program NQENDFIT available. The writing of this paper was facilitated by a travel scholarship to A.S., granted by the Nordic Academy for Advanced Study (NorFA), and by support from the Norwegian Research Council. Y.I. and A.L. acknowledge support from the Swedish Foundation for International Cooperation in Research and Higher Education (STINT) and the Swedish Natural Science Research Council.

Appendix A

By describing the electron orbitals at a carbon atom located a distance R from the quadrupole using Slater orbitals, it is possible to calculate the contribution to each element of the quadrupolar coupling tensor, Q_{ij}, from every electron. The necessary integrals for doing this are given below.

The Slater orbitals are given by

$$|1s\rangle = \left(\frac{\zeta^3}{\pi}\right)^{1/2} e^{-\rho} \qquad |2p_x\rangle = \left(\frac{\zeta^3}{\pi}\right)^{1/2} \rho e^{-\rho} \cos\theta$$

$$|2s\rangle = \left(\frac{\zeta^3}{3\pi}\right)^{1/2} \rho e^{-\rho} \qquad |2p_y\rangle = \left(\frac{\zeta^3}{\pi}\right)^{1/2} \rho e^{-\rho} \sin\theta \cos\phi \quad (9)$$

$$|2p_z\rangle = \left(\frac{\zeta^3}{\pi}\right)^{1/2} \rho e^{-\rho} \sin\theta \cos\phi$$

where $\zeta = Z^*/a_0 n$ and $\rho = \zeta r$, with Z^* being the effective nuclear charge, n the principal quantum number, and a_0 the Bohr radius.

The coordinates used in the calculations are defined in Figure 5, with the z axis along the $D-C_0$ bond and the x axis parallel to the LEO. The Cartesian coordinates with origin at D, expressed by (r, θ, ϕ), defined as the polar coordinates with origin at the nucleus at which the orbital is centered, are

$$x = \frac{\rho}{\zeta} \sin\theta \cos\phi$$

$$y = \frac{\rho}{\zeta} \sin\theta \sin\phi \quad (10)$$

$$z = \frac{1}{\zeta}(2a + \rho \cos\theta)$$

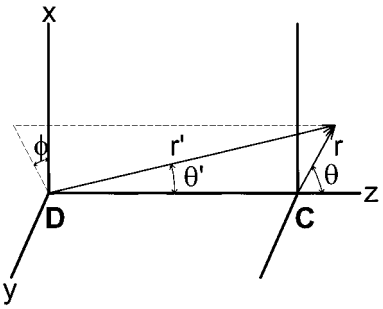

Figure 5. Coordinates used for calculating the quadrupolar coupling for an α-deuteron. The Slater orbitals have polar coordinates (r, θ, ϕ) in a coordinate system centered on the carbon atom, whereas (r', θ', ϕ) are the polar coordinates centered on the deuteron.

With $a = \zeta R$, where R is the bond length between D and C_0, and with the definition $P_{ij}(r) = (3x_ix_j - \delta_{ij}r^2)/r^5$, the results for the integrals are

$$\langle 1s|P_{zz}(r)|1s\rangle = -\frac{2}{R^3}[e^{-2a}(2a^2 + 2a + 1) - 1] \quad (11)$$

$$\langle 1s|P_{xx}(r)|1s\rangle = \langle 1s|P_{yy}(r)|1s\rangle = -\frac{1}{2}\langle 1s|P_{zz}(r)|1s\rangle \quad (12)$$

$$\langle 2s|P_{zz}(r)|2s\rangle = -\frac{2}{R^3}\left[e^{-2a}\left(\frac{2}{3}a^4 + \frac{4}{3}a^3 + 2a^2 + 2a + 1\right) - 1\right] \quad (13)$$

$$\langle 2s|P_{xx}(r)|2s\rangle = \langle 2s|P_{yy}(r)|2s\rangle = -\frac{1}{2}\langle 2s|P_{zz}(r)|2s\rangle \quad (14)$$

$$\langle 2p_x|P_{xx}(r)|2p_x\rangle = \frac{1}{R^3}\left[\frac{27}{2a^2} - 1 - e^{-2a}\left(2a^3 + 7a^2 + 16a + 26 + \frac{27}{a} + \frac{27}{2a^2}\right)\right] \quad (15)$$

$$\langle 2p_x|P_{yy}(r)|2p_x\rangle = \frac{1}{R^3}\left[\frac{9}{2a^2} - 1 - e^{-2a}\left(a^2 + 4a + 8 + \frac{9}{a} + \frac{9}{2a^2}\right)\right] \quad (16)$$

$$\langle 2p_x|P_{zz}(r)|2p_x\rangle = -(\langle 2p_x|P_{xx}(r)|2p_x\rangle + \langle 2p_x|P_{yy}(r)|2p_x\rangle) \quad (17)$$

$$\langle 2p_y|P_{xx}(r)|2p_y\rangle = \langle 2p_x|P_{yy}(r)|2p_x\rangle$$
$$\langle 2p_y|P_{yy}(r)|2p_y\rangle = \langle 2p_x|P_{xx}(r)|2p_x\rangle \quad (18)$$
$$\langle 2p_y|P_{zz}(r)|2p_y\rangle = \langle 2p_x|P_{zz}(r)|2p_x\rangle$$

$$\langle 2p_z|P_{zz}(r)|2p_z\rangle = -\frac{2}{R^3}\left[e^{-2a}\left(2a^4 + 6a^3 + 14a^2 + 26a + 37 + \frac{36}{a} + \frac{18}{a^2}\right) - \frac{18}{a^2} - 1\right] \quad (19)$$

$$\langle 2p_z|P_{xx}(r)|2p_z\rangle = \langle 2p_z|P_{yy}(r)|2p_z\rangle = -\frac{1}{2}\langle 2p_z|P_{zz}(r)|2p_z\rangle \quad (20)$$

$$\langle 2s|P_{zz}(r)|2p_z\rangle = -\frac{2}{\sqrt{3}R^3}\left[\frac{15}{2a} - \left(2a^4 + 5a^3 + 10a^2 + 16a + 15 + \frac{15}{2a}\right)e^{-2a}\right] \quad (21)$$

$$-\frac{1}{2}\langle 2s|P_{zz}(r)|2p_z\rangle = \langle 2s|P_{xx}(r)|2p_z\rangle = \langle 2s|P_{yy}(r)|2p_z\rangle = \langle 2s|P_{zx}(r)|2p_x\rangle = \langle 2s|P_{zy}(r)|2p_y\rangle \quad (22)$$

$$\langle 2p_x|P_{xy}(r)|2p_y\rangle = -\frac{1}{R^3}\left[\left(a^3 + 3a^2 + 6a + 9 + \frac{9}{a} + \frac{9}{2a^2}\right)e^{-2a} - \frac{9}{2a^2}\right] \quad (23)$$

$$\langle 2p_x|P_{xz}(r)|2p_z\rangle = \frac{1}{R^3}\left[\left(2a^4 + 5a^3 + 12a^2 + 24a + 36 + \frac{36}{a} + \frac{18}{a^2}\right)e^{-2a} - \frac{18}{a^2}\right] \quad (24)$$

$$\langle 2p_y|P_{yz}(r)|2p_z\rangle = \langle 2p_x|P_{xz}(r)|2p_z\rangle \quad (25)$$

References and Notes

(1) McConnell, H. M.; Heller, C.; Cole, T.; Fessenden, R. W. *J. Am. Chem. Soc.* **1960**, *82*, 766.
(2) Colligiani, A.; Pinzino, C.; Brustolon, M.; Corvaja, C. *J. Magn. Reson.* **1978**, *32*, 419.
(3) Colligiani, A.; Pinzino, C.; Brustolon, M.; Corvaja, C.; Bandoli, G.; Clemente, D. A. *Mol. Phys.* **1980**, *39*, 1153.
(4) McCalley, R. C.; Kwiram, A. L. *J. Phys. Chem.* **1993**, *97*, 2888.
(5) Sagstuen, E.; Lund, A.; Itagaki, Y.; Maruani, J. *J. Phys. Chem. A* **2000**, *104*, 6362.
(6) McConnell, H. M.; Chesnut, D. B. *J. Chem. Phys.* **1958**, *28*, 107.
(7) McConnell, H. M.; Strathdee, J. *Mol. Phys.* **1959**, *2*, 129.
(8) Wells, J. W. *J. Chem. Phys.* **1977**, *66*, 632.
(9) Goslar, J.; Piekara-Sady, L.; Kispert, L. D. ENDOR Data Tabulations. In *Handbook of Electron Spin Resonance*; Poole, J. C. P., Farach, H. A., Eds.; AIP Press: Woodbury, NY, 1994; p 360.
(10) Colligiani, A.; Pinzino, C.; Brustolon, M.; Corvaja, C. *J. Magn. Reson.* **1980**, *41*, 279.
(11) McCalley, R. C.; Kwiram, A. L. *Phys. Rev. Lett.* **1970**, *24*, 1279.
(12) Dalton, L. R.; Kwiram, A. L. *J. Am. Chem. Soc.* **1972**, *94*, 6930.
(13) Krzystek, J.; Kwiram, A. B.; Kwiram, A. L. *J. Phys. Chem.* **1995**, *99*, 402.
(14) Moulton, G. C.; Coleman, J. M. *J. Chem. Phys.* **1984**, *80*, 4648.
(15) Pöppl, A.; Völkel, G.; Tober, O.; Klöpperpieper, A.; Hüttermann, J.; Gatzweiler, W. *Chem. Phys.* **1993**, *171*, 375.
(16) Goedkoop, J. A.; MacGillavry, C. H. *Acta Crystallogr.* **1957**, *10*, 125.
(17) Busing, W. R.; Martin, K. O.; Levy, H. A. Report ORNL-TM-306; Oak Ridge National Laboratories: Oak Ridge, TN, 1964.
(18) Thuomas, K.-Å.; Lund, A. *J. Magn. Reson.* **1975**, *18*, 12.
(19) Sørnes, A. R.; Sagstuen, E.; Lund, A. *J. Phys. Chem.* **1995**, *99*, 16867.
(20) Pople, J. A.; Beveridge, D. L. *Approximate Molecular Orbital Theory*; McGraw-Hill: New York, 1970.
(21) Oloff, H.; Hüttermann, J. *J. Magn. Reson.* **1980**, *40*, 415.
(22) Frisch, M. J.; Trucks, G. W.; Schlegel, H. B.; Scuseria, G. E.; Robb, M. A.; Cheeseman, J. R.; Zakrewski, V. G.; Montgomery, J. A., Jr.; Stratmann, R. E.; Burant, J. C.; Dapprich, S.; Millam, J. M.; Daniels, A. D.; Kudin, K. N.; Strain, M. C.; Farkas, O.; Tomasi, J.; Barone, V.; Cossi, M.; Cammi, R.; Mennucci, B.; Pomelli, C.; Adamo, C.; Clifford, S.; Ochterski, J.; Petersson, G. A.; Ayala, P. Y.; Cui, Q.; Morokuma, K.; Malick, D. K.; Rabuck, A. D.; Raghavachari, K.; Foresman, J. B.; Cioslowski, J.; Ortiz, J. V.; Stefanov, B. B.; Liu, G.; Liashenko, A.; Piskorz, P.; Komaromi, I.; Gomperts, R.; Martin, R. L.; Fox, D. J.; Keith, T.; Al-Laham, M. A.; Peng, C. Y.; Nanayakkara, A.; Gonzalez, C.; Challacombe, M.; Gill, P. M. W.; Johnson, B. G.; Chen, W.; Wong, M. W.; Andres, J. L.; Head-Gordon, M.; Replogle, E. S.; Pople, J. A. *Gaussian 98*, revision A.4; Gaussian, Inc.: Pittsburgh, PA, 1998.
(23) Bonazzola, L.; Hesse-Bezot, C.; Leray, N.; Roncin, J. *J. Magn. Reson.* **1973**, *12*, 280.
(24) Benetis, N. P., Dept. Phys. Meas. Tech., Univ. Linköping, Sweden, 1997.
(25) Salih, N. A.; Eid, O.; Benetis, N. P.; Lindgren, M.; Lund, A.; Sagstuen, E. *Chem. Phys.* **1996**, *212*, 409.
(26) Atherton, N. M. *Principles of Electron Spin Resonance*; Ellis Horwood PTR Prentice Hall: London, 1993.
(27) Townes, C. H.; Dailey, B. P. *J. Chem. Phys.* **1949**, *17*, 782.
(28) Barfield, M. *J. Chem. Phys.* **1970**, *53*, 3836.
(29) Beveridge, D. L.; McIver, J. W., Jr. *J. Chem. Phys.* **1971**, *54*, 4681.
(30) Edlund, O.; Lund, A.; Shiotani, M.; Sohma, J.; Thuomas, K.-Å. *Mol. Phys.* **1976**, *32*, 49.
(31) Karplus, M.; Fraenkel, G. K. *J. Chem. Phys.* **1961**, *35*, 1312.
(32) Sagstuen, E.; Awadelkarim, O.; Lund, A.; Masiakowski, J. *J. Chem. Phys.* **1986**, *85*, 3223.
(33) Weil, J. A.; Rao, P. S. *Bruker EPR/ENDOR Frequency Table*; Bruker: Karlsruhe, Germany, 1998.
(34) McConnell, H. M. *J. Chem. Phys.* **1958**, *24*, 764.
(35) Fessenden, R. W.; Schuler, H. *J. Chem. Phys.* **1963**, *39*, 2147.
(36) McDowell, C. A.; Naito, A. *J. Magn. Reson.* **1981**, *45*, 205.